Dynamics of an unusual cone-building trachyte eruption at Pu‘u Wa‘awa‘a, Hualālai volcano, Hawaii

by Thomas Shea, Tanis Leonhardi, Thomas Giachetti, Amanda Lindoo, Jessica Larsen, John Sinton, Elliott Parsons

SUPPLEMENTARY MATERIAL

1. Feldspar compositions

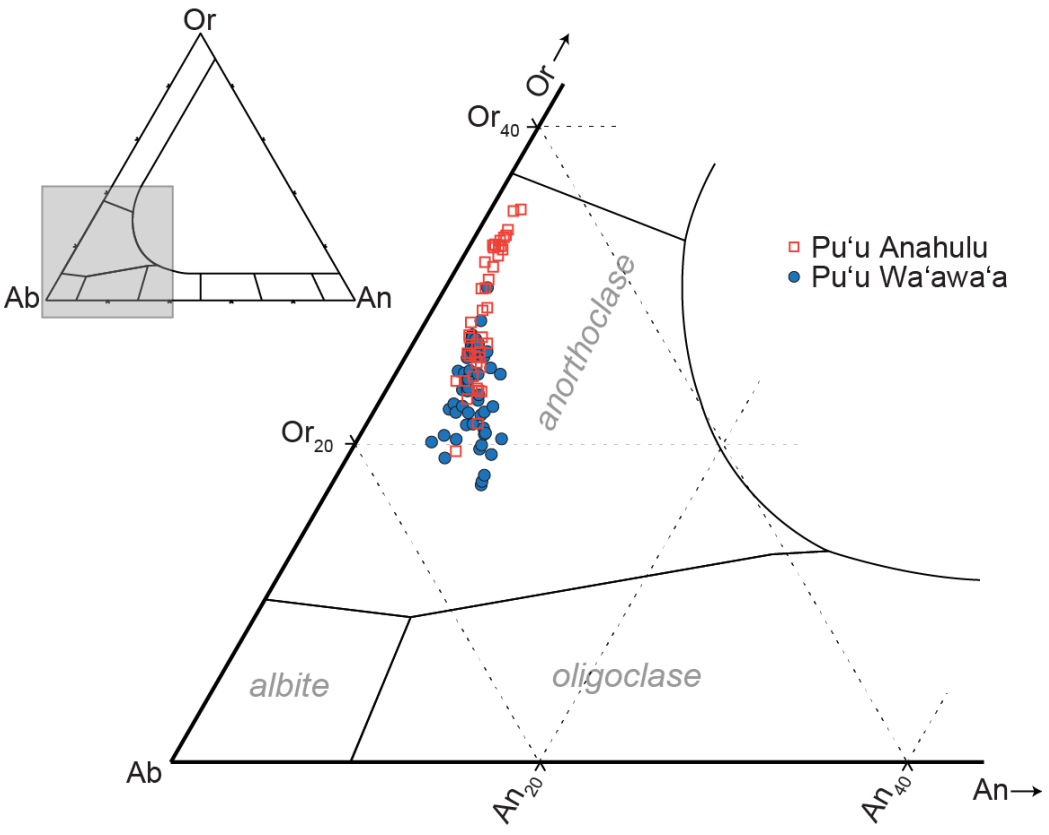

Fig. A1 Composition of feldspar microlites and microphenocrysts in the Pu’u Wa‘awa‘a and Pu‘u Anahulu trachytes. Despite the significant overlap, Pu‘u Anahulu feldspars are slightly richer in orthoclase.

2. Textural heterogeneity at the single clast scale

Figure A2 shows examples of textural variations observed in the PWW pyroclasts. See text for details.

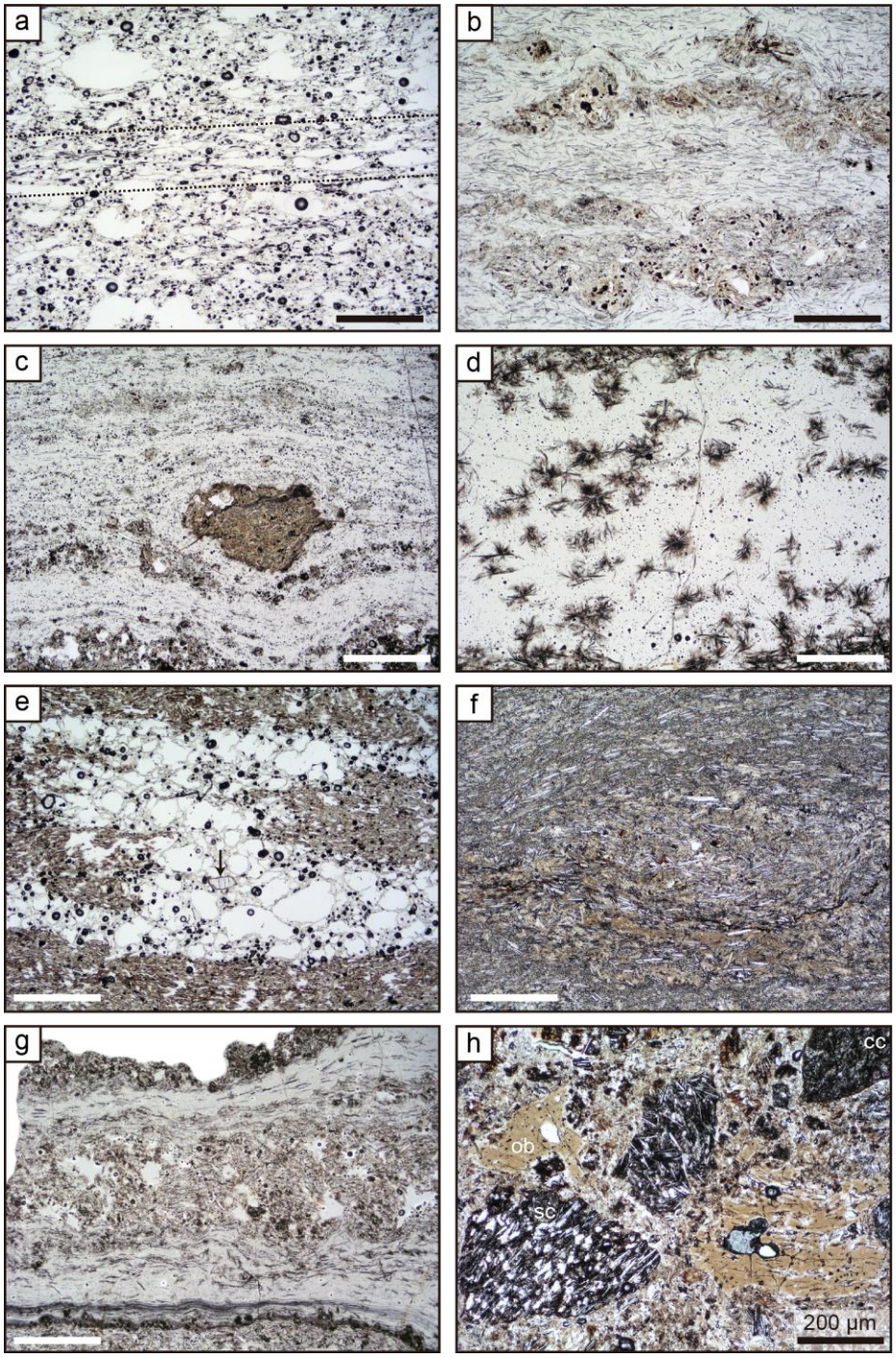

Fig. A2 Photomicrogaphs of clast-scale textural heterogeneities within Pu'u Wa'awa'a pyroclasts. (a) Localized shear-zone (region bound by dotted lines) marked by elongate vesicles within a pumice clast. (b) Disaggregated and stretched crystal-rich regions within a microlite-bearing obsidian. Note clear preferential microlite orientation. (c) Cryptocrystalline inclusion ("Augen" texture) in banded obsidian. (d) Microspherulites in banded obsidian. (e) Pumiceous band within scoriaceous clast. Arrows shows resorbed olivine crystal. (f) Recumbent microfold structure within cryptocrystalline clast. (g) Highly heterogeneous clast with vesicular, scoriaceous bands and thin microlite foliation. (h) Breccia clast with domains of obsidian, scoriaceous and/or cryptocrystalline inclusions surrounded by agglutinated glass shards (matrix). Scale bars represent 250 µm except for h.

3. Rehydration in the PWW pyroclasts

Methods

MicroRaman H_2O profiles and maps

In addition to the spot analyses presented in the main text, two additional transects and a map were acquired within one obsidian sample close to the clast edge to check for potential heterogeneity associated with rehydration rinds (e.g. Friedman et al. 1966). A green laser (532 nm) was used at maximum power (20 mW), three accumulations of 20 s dwell times were completed for spots and transects, while mapping was done using single dwell times of 4 s per grid point. Spectrum baselines were subtracted separately in the ASF and H_2O_t wavenumber regions via polynomial fits, using the SpeCTRa Matlab-based program. The obtained baseline-corrected intensities were corrected for acquisition temperature using the Long equation (Le Losq et al. 2012) and the ASF and H_2O_t band areas integrated for quantification.

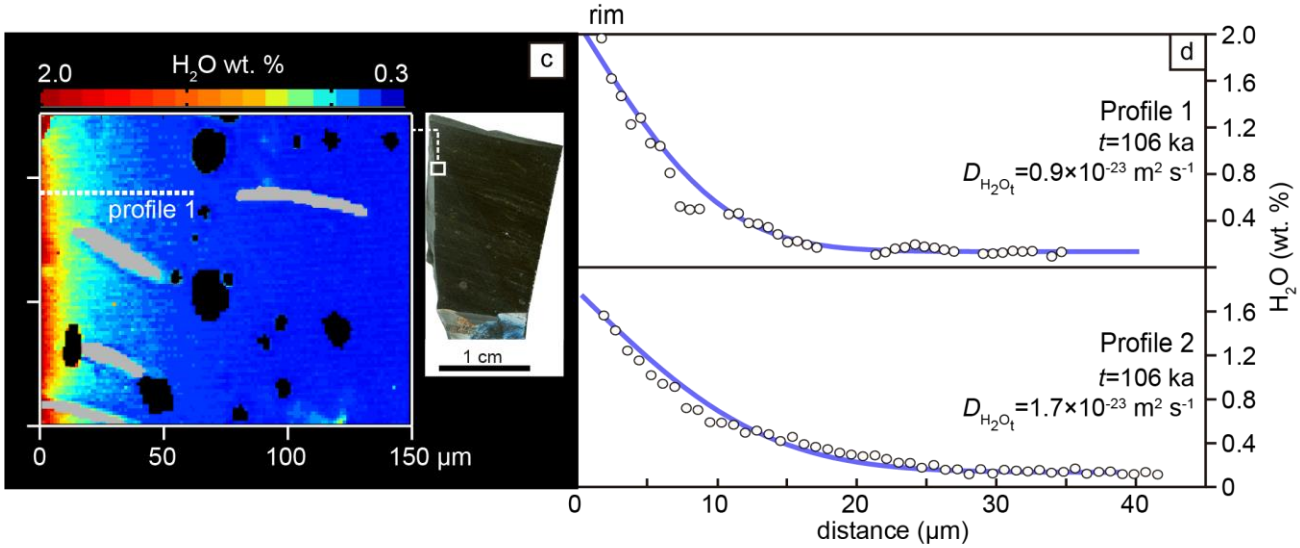

Fig. A3 H_2O map and profiles within the edge of a Pu'u Wa'awa'a obsidian clast (gray areas in the Raman map are anorthoclase). There is a clear meteoric rehydration rind, which can be used to estimate effective H_2O diffusivities at ambient temperature (~20°C) assuming the total rehydration period (106 ka, Clague 1987).

Thermogravimetric Analysis

Details of the technique are reported in Giachetti et al. (2015). Briefly, texturally homogeneous samples - or homogeneous domains within banded samples - were crushed and sieved to preserve only grains <53 µm, 15-45 mg of which were placed in a tared alumina cup and inserted in a TA Instruments Q500 Thermogravimetric Analyzer at Rice University. Samples were heated by 20 °C increments from room temperature to 1000 °C under an oxygen-free environment, and their mass monitored every 0.5 s. The mass lost during these analyses is inferred to be dominantly water, with potentially some other elements such as Cl or F that can escape at the highest temperatures (cf. Shea et al. 2014). The results of TGA are expressed in the form of temperature vs. mass loss (or the derivative of mass loss), allowing

visualization of volatile escape patterns that may be used to decipher meteoric from magmatic water (Denton et al. 2012; Giachetti et al. 2015).

Results

The microRaman water map acquired within the edge of an obsidian sample (i.e. portion of clast in contact with atmosphere) shows a clear ~20-30 micron thick enrichment at the rind (Fig. A3). This feature is characteristic of meteoric rehydration rinds, which can be used for archeological dating (Friedman et al. 1966; Anovitz et al. 2006). Two detailed transects across different obsidian pyroclasts were also performed to verify whether the rims recorded a similar enrichment. The profiles are similar in shape despite attaining slightly different maximum values of H_2O_{tot} at the edge (Fig. A3). Assuming that these profiles represent post-eruption rehydration by meteoric water, the majority of the water measured in vesicular clasts (i.e. >40% vol., Fig. 10a in the main text) is likely secondary rather than magmatic.

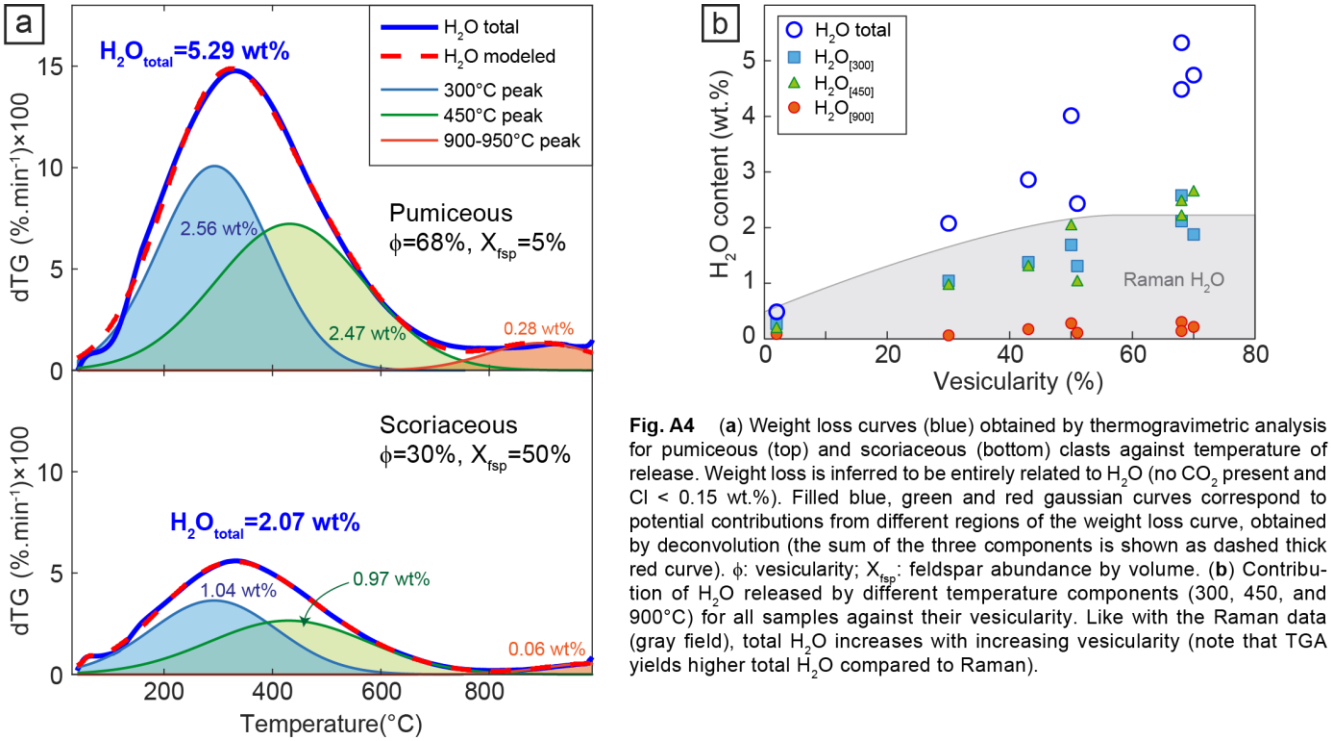

Fig. A4 (**a**) Weight loss curves (blue) obtained by thermogravimetric analysis for pumiceous (top) and scoriaceous (bottom) clasts against temperature of release. Weight loss is inferred to be entirely related to H_2O (no CO_2 present and Cl < 0.15 wt.%). Filled blue, green and red gaussian curves correspond to potential contributions from different regions of the weight loss curve, obtained by deconvolution (the sum of the three components is shown as dashed thick red curve). ϕ: vesicularity; X_{fsp}: feldspar abundance by volume. (**b**) Contribution of H_2O released by different temperature components (300, 450, and 900°C) for all samples against their vesicularity. Like with the Raman data (gray field), total H_2O increases with increasing vesicularity (note that TGA yields higher total H_2O compared to Raman).

Weight loss vs. temperature curves ("dTG") acquired by TGA are used to estimate bulk total volatile content (Roulia et al. 2006). The dTG curves obtained for Pu'u Wa'awa'a clasts representing three textural end-members (pumiceous, scoriaceous and obsidian) are all uni- or bimodal, with a dominant degassing peak at T=0-800 °C and a small secondary peak at T>800 °C (Fig. A4a). The dominant lower temperature peak is inferred to represent loss of weakly-bonded molecular H_2O, whereas the high temperature peak usually corresponds to loss of more strongly-bonded OH species (e.g. Giachetti et al. 2015). The main peak is asymmetric and can be further deconvoluted into two Gaussian curves, centered on T=300 °C and T=450 °C (Fig. A4a). Assuming that weight loss is dominated by H_2O volatilization, the total H_2O contents integrated under the dTG curves show a clear

increase with sample vesicularity (~0.4 wt. % for vesicle-free obsidian and ~5 wt. % for pumiceous clasts). If the low temperature T=300°C region represents dominantly loosely bonded meteoric water, then at least half of the total H_2O in these samples comes from post-eruptive rehydration (Fig. A4b). The T=900 °C region is likely associated with OH groups, and we infer that the intermediate regions (T=450 °C) represent partly magmatic and partly meteoric molecular H_2O.

The total water contents are nearly double the H_2O_{total} measured by Raman. Possibly, the ~1 μm spots measured by Raman are far enough from vesicle walls, where rehydration effects are highest, so that very variable H_2O concentrations are measured, particularly in vesicular samples (Fig. 10a in the main text). In comparison, TGA is a bulk technique and better characterizes the extent of rehydration for the entire sample.

Modeling rehydration rates

Overall, both microRaman and TGA analyses suggest that H_2O enrichment rinds in PWW obsidian are related to meteoric rehydration. Under this premise, we can use a simple 1D diffusion model employing a constant integrated H_2O_t diffusivity to fit the microRaman H_2O profiles (Fig. A3). Best fits are produced for $D_{H2Ot} = 0.9\text{-}1.7\times10^{-23}$ m^2 s^{-1}, which are within the lower range inferred for water diffusion at ambient temperature for rhyolites (Giachetti and Gonnermann 2013), and agree with values obtained by Liritzis et al. (2004, 2008) and Laskaris et al. (2011) using secondary ionization mass spectrometry techniques on natural obsidian from different environments. Diffusion of H_2O at ambient temperature may, however, be concentration dependent (e.g. Ni and Zhang 2008) so that such values only represent effective diffusivities over extended periods.

4. Increase in Fe3+ content within microcrystalline and scoriaceous clasts

Figure A5 shows three Raman spectra acquired in texturally different samples, illustrating that the more crystalline samples likely resided in the shallow conduit for longer periods of time and oxidized.

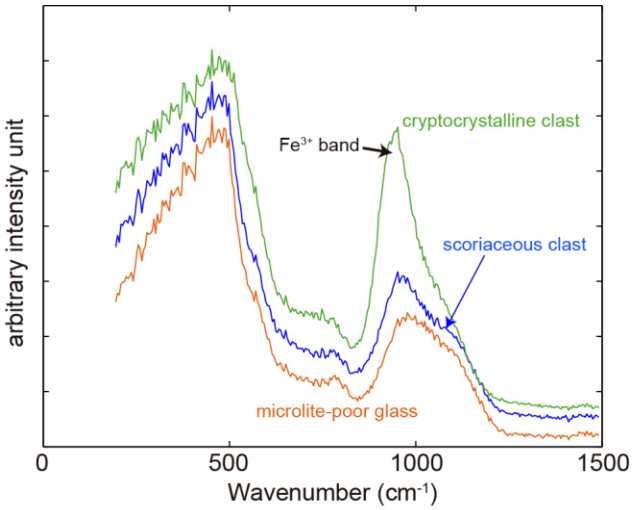

Fig. A5 Low frequency portion of the Raman spectrum for three different Pu'u Wa'awa'a glasses. The band around 980cm^{-1} corresponds to an $Fe^{3+}O_4$-SiO_4 vibration mode. The influence of Fe^{3+} is stronger in scoriaceous and cryptocrystalline clasts than in microlite-poor glasses (pumice or obsidian), suggesting oxidation.

5. Same-scale comparison of PWW cone dimensions with other cinder/tephra cones

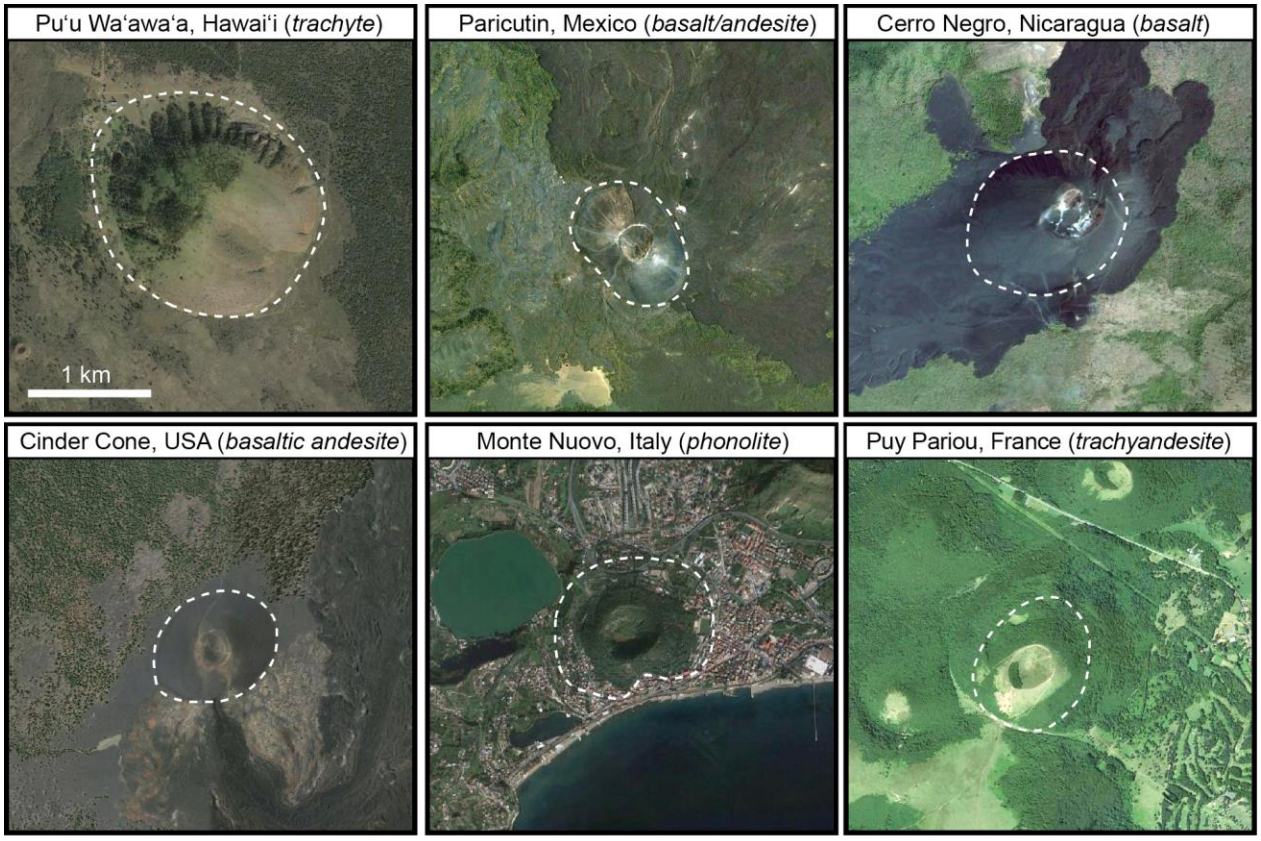

Fig. A6 Comparison between Pu'u Wa'awa'a and other well-studied tephra cones around the world. The eruptions that produced these constructs are inferred to have been 'violent strombolian' in style for at least part of their life cycles, which in some cases likely lasted months to several years (e.g. Paricutin) or spanned several episodes over decades (e.g. Cerro Negro). All images have the same scale

6. MELTS-generated phase equilibria diagram for the PWW trachyte

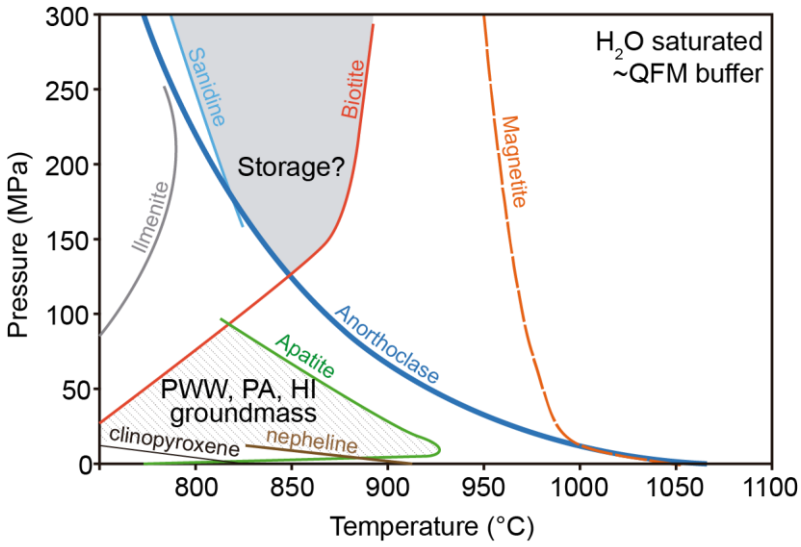

Fig. A7 MELTS-simulated phase equilibria for a Hualalai trachyte composition. Grayed area shows potential storage conditions assuming that biotite and magnetite are stable as a phenocryst phases with no feldspar present. Dashed area corresponds to groundmass assemblage.